atmosphere

MDPI

Article

Non-Negligible Factors Influence Tree-Ring-Based Temperature Reconstruction and Comparison over Mid-Latitude China

Zeyu Zheng [1,2], Zhenqian Wang [3,4,*] and Yufang Zhang [5]

[1] Tourism Department, Guangzhou City Polytechnic, Guangzhou 510405, China; zhengzy17@lzu.edu.cn
[2] MOE Key Laboratory of Western China's Environmental System, College of Earth and Environmental Sciences, Lanzhou University, Lanzhou 730000, China
[3] School of Atmospheric Sciences, Lanzhou University, Lanzhou 730000, China
[4] Department of Physical Geography and Bolin Centre for Climate Research, Stockholm University, 10691 Stockholm, Sweden
[5] Sichuan Provincial Agricultural Meteorological Center, Chengdu 610072, China; yufang918@sina.com
* Correspondence: zhenqian.wang@natgeo.su.se

Abstract: Warm-season mean maximum temperature changes over mid-latitude regions have been attracting increasing attention amid the background of global warming. In this study, we present three tree-ring width chronologies: Tongbai Mountain (TBM; 1916–2014), Shimen Mountain (SMM; 1663–2014), and Xinlong (XL; 1541–2014), derived respectively from the eastern Qinling Mountains, north–central China, and the eastern Tibetan Plateau. Therein, TBM and SMM are newly developed, while XL is a reanalysis. Correlation analysis with climatic factors reveals that these three chronologies exhibit the highest correlation with the May–July mean maximum temperature. Based on these chronologies, we conducted reconstructions of the May–July mean maximum temperature. Spatial correlation analysis of each reconstruction with concurrent observed data, as well as comparisons with nearby temperature reconstructions, indicates their large-scale representativeness. However, during the common period of 1916–2014, the three chronologies show weak correlations with each other at the interannual timescale. Furthermore, the 11-year running correlation coefficients among the three reconstructions fluctuated during this common period. Additionally, fluctuations were observed between the reconstructions from SMM and XL during the overlapping period of 1668–2009, suggesting that tree-ring-based temperature reconstructions may be inconsistent when compared over mid-latitude China. These inconsistent changes can be attributed to the regional differences in the May–July mean maximum temperature change, the influence of different precipitation signals on the maximum temperature, and the El Niño–Southern Oscillations.

Keywords: dendrochronology; mean maximum temperature; comparison; El Niño–Southern Oscillations; mid-latitude China

Academic Editors: Jason T. Ortegren and Gareth Marshall

Received: 5 December 2024
Revised: 7 January 2025
Accepted: 17 January 2025
Published: 27 January 2025

Citation: Zheng, Z.; Wang, Z.; Zhang, Y. Non-Negligible Factors Influence Tree-Ring-Based Temperature Reconstruction and Comparison over Mid-Latitude China. *Atmosphere* **2025**, *16*, 137. https://doi.org/10.3390/atmos16020137

1. Introduction

Temperatures have been significantly increasing in recent decades. According to the IPCC 6th assessment report, the average global surface temperature has risen by approximately 1.1 °C during the period 2011–2020 and will continue to rise in both the 21st and 22nd centuries under different climate change predictions [1]. In recent decades, the mid and high latitudes of the Northern Hemisphere have experienced the warmest years during the period of instrumental measurements, which has induced a series of environmental problems such as land degradation and glacier retreat [2–4]. Previous studies suggested that significant warming occurred at minimum temperatures and at

night in most regions of the Northern Hemisphere [5]. However, the increased frequency of extreme warm events in the warm season, which is relevant to the maximum temperature and directly affects people's lives, is worth heeding. For example, summer heatwaves and hot spells have occurred in all parts of Europe and East Asia in recent years, causing severe death and economic losses, especially in 1995, 2003, and 2022 [6–8]. Therefore, more attention has been paid to the warm-season mean maximum temperature [9], especially in mid-latitude China, which accounts for 60% or more of its area and is sensitive to climate change because it stretches across different climate types [10,11].

The establishment of most meteorological stations in mainland China occurred after the 1950s [12,13], resulting in limited instrumental records in both time and space. This limitation hinders our ability to detect the maximum temperature change over longer timescales. In recent decades, tree rings have been widely used to reconstruct mean maximum temperature variations, as they are one of the most high-resolution and widespread sources of past environmental information [14,15]. For example, Sun et al. [16] and Liu et al. [15] reconstructed the maximum warm-season temperature in northeastern China. Tian et al. [17] presented May–July maximum temperature reconstruction in east–central China. Chen et al. [18] reconstructed the April-August maximum temperature change in western China. These investigations further emphasize the potential of tree rings for maximum temperature reconstructing and enhance our understanding of mean maximum temperature change at interannual to decadal timescales.

Furthermore, some of the studies further utilize the synthetic chronology to detect regional temperature change. For example, Duan et al. [19] reported a regional-scale winter–spring temperature reconstruction based on five tree-ring chronologies in southeastern China. Li et al. [20] extracted the common signal from five tree-ring chronologies to reconstruct the regional temperature in the north of the Western Sichuan Plateau. Keyimu et al. [21] synthesized 22 chronologies to reconstruct the minimum temperature change in the southeast of the Tibetan Plateau. Chronologies for synthesizing were selected either in close locations or as temperature-sensitive based on their correlation with monthly temperature records from the nearest meteorological stations. However, considering the complicated topography and hydrothermal conditions over mid-latitude China, some of the temperature reconstructions derived from the same region showed significant differences with each other. For example, the comparison among the temperature reconstructions in the Qinling Mountains, an important geographic demarcation line in central mainland China, where the tree growth is known to be sensitive mainly to the early spring and early summer temperatures, showed that variations of the early spring and early summer temperatures were out of phase in the past [22,23]. Furthermore, the influence of large-scale atmospheric circulations, such as the El Niño–Southern Oscillations (ENSO), is itself a complex physical process and is inconsistently associated with local conditions [24]. Therefore, it is necessary to develop additional mean maximum temperature reconstructions at the regional scale. Furthermore, the possible factors influencing tree-ring-based temperature reconstruction and comparison over mid-latitude China are worth investigating. Therefore, the objectives of this study were to (1) reconstruct the past mean maximum temperature variations based on tree-ring width chronologies in mid-latitude China, (2) analyze and compare these reconstructions with existing reconstructions, and (3) identify possible factors influence tree-ring-based temperature reconstruction and comparison over mid-latitude China.

2. Materials and Methods

2.1. Study Area Characteristics

The sites included Tongbai Mountain (TBM), Shimen Mountain (SMM), and Xinlong (XL). Both TBM and SMM are being presented here for the first time in this study. A

study on XL was previously published [25]. As shown in Figure 1, the TBM is located in the eastern Qinling Mountains (QLMs). According to the local meteorological station, Nanyang Station record, the annual mean temperature and total precipitation range from 13.97 °C to 16.67 °C and 509 mm to 1290 mm, respectively, which indicates that the regional climate is humid [26]. The SMM is located on the northern slope of the western QLMs and adjoins the Loess plateau to the north. This area is considered a transitional zone between arid and humid regions, with the annual mean temperature and total precipitation ranging from 9.86 °C to 12.89 °C and 321 mm to 809 mm, respectively [27]. XL is located on the southeastern Tibetan Plateau (TP), where the annual mean temperature is 6.7 °C and the multi-year mean annual total precipitation is 601 mm for 1951–2019 [25]. Furthermore, the summer precipitation (June–August) at these three sample sites constituted over half of the total annual rainfall, with the peak of warm and wet conditions occurring in July, showcasing a characteristic monsoonal climate.

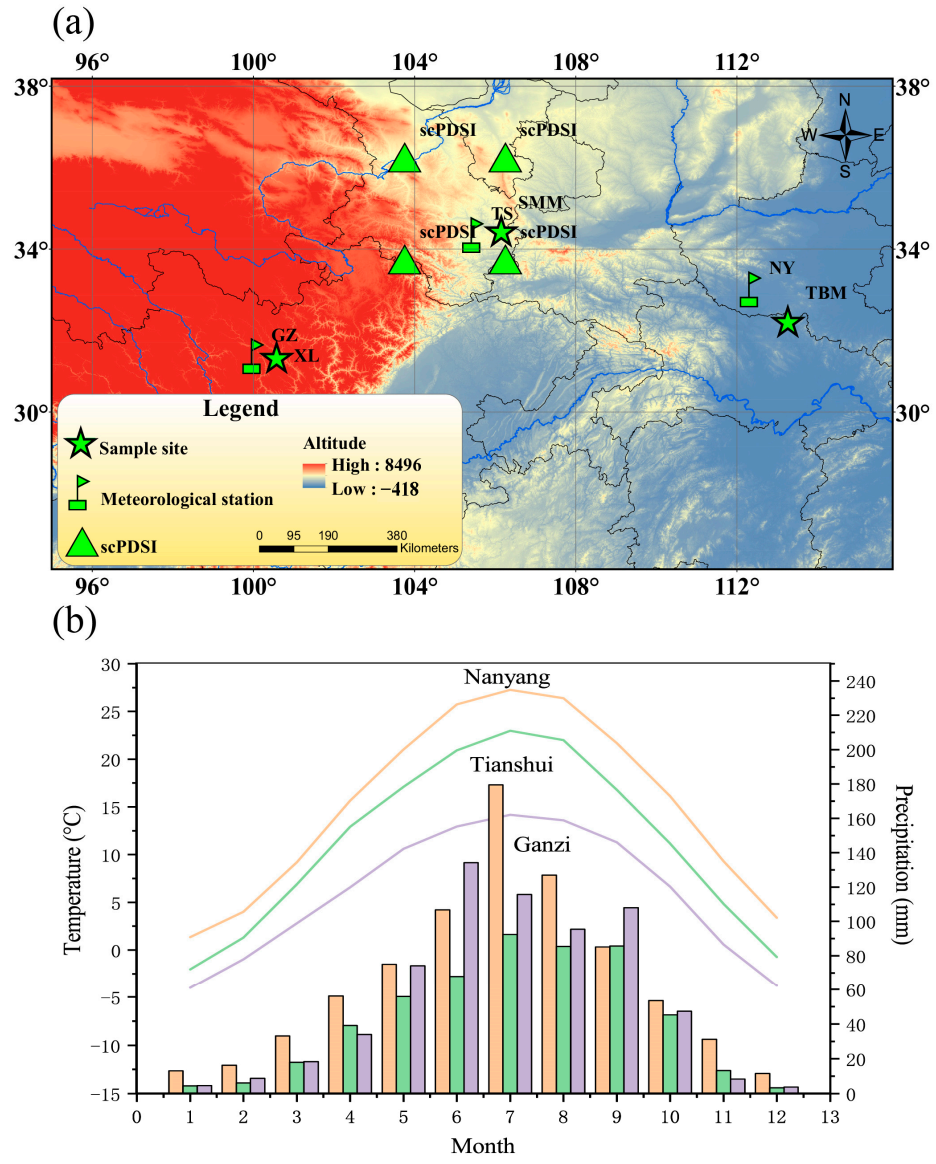

Figure 1. (**a**) Location of the sampling site and corresponding meteorological stations. (**b**) Monthly mean and monthly total precipitation were calculated using climate data from Nanyang (orange), Tianshui (green), and Ganzi (purple) during the periods 1954–2019, 1953–2019, and 1951–2019, respectively.

2.2. Tree-Ring Data and Chronology Development

Following the technique for acquiring tree-ring width data and ensuring quality control in dendroclimatological research [28], more than 20 living elder trees from each sample site were collected from trees at breast height (1.3 m above the ground) using a 10 mm increment to ensure the length and quality of cross-dating. The dominant tree species with distinct annual rings and sensitive responses to climate change were chosen for research. Additionally, the sample sites with less human activity and a stable natural environment were selected. In 2018, a total of 48 cores were collected from 24 living *Pinus tabulaeformis* trees within an altitude range of 1650–1820 m a.s.l. in the SMM Nature Reserve (34.45° N, 106.15° E). In 2019, 46 cores were obtained from 31 *Picea balfouriana* trees in XL county (31.35° N, 100.58° E, 3880 m a.s.l.) in the southeastern TP. In 2020, 47 cores were sampled from 26 *Pinus massoniana* trees at TBM (32.4° N, 113.27° E), located at approximately 500 m a.s.l. in east–central China. Further details can be found in Table 1.

Table 1. Statistics of the tree-ring sampling sites, the nearest meteorological station, and the scPDSI grid points.

Data Type	Site Code	Latitude	Longitude	Elevation (m a.s.l.)	Number	Slopes	Species
Tree-ring	TBM	32.24	113.27	680	25/47	20–30%	*Pinus massoniana*
	SMM	34.45	106.15	2210	20/40	30–40%	*Pinus tabulaeformis*
	XL	31.35	100.58	3880	31/46	30–40%	*Picea balfouriana*
Meteorological data	NY	33.02	112.35	129.2			
	TS	34.35	105.45	1141.6			
	GZ	31.37	100	3393.5			
scPDSI		33.75° N–36.25°N	103.75° E–106.25° E				

Pre-treatments were conducted according to the standard procedure for analyzing tree rings. First, all core samples were mounted, dried, and sanded [29]. Then, an optical microscope was employed for preliminary dating. Next, the ring widths were precisely measured with a resolution of 0.001 mm using a Velmex ring width measuring system. Once the measurements were completed, the computer program COFECHA (Version 6.03P) was utilized for quality control purposes to verify the cross-dating [30]. Subsequently, the raw ring widths were detrended using negative exponential curves and a cubic smoothing spline with a 50% frequency response cutoff equal to 67% of the series length. Finally, ARSTAN was employed to obtain the standard chronology (STD), residual chronology (RES), and autoregression chronology (ARS) [31]. Among the three chronologies, STD was chosen for further investigation due to its ability to retain low-frequency signals effectively [24,32]. The pertinent statistical characteristics of the standard tree-ring chronology can be found in Table 2, along with the statistical data related to subsample signal strength (SSS), which was selected with a threshold value of 0.85 to determine the reliable period (Figure 2) [33]. Since the TBM was set as a tourist area in 2014, the growth of trees there has been remarkably influenced by the increasing intensity of human activities. Given that the purpose of this study was to detect possible factors influencing tree-ring-based temperature reconstruction and comparison over mid-latitude China, all the analyses are therefore based on data up to 2014.

Table 2. Statistical characteristics of the chronologies.

Statistical Item	TBM Chronology	SMM Chronology	XL Chronology
Standard deviation (SD)	0.351	0.338	0.321
Mean sensitivity (MS)	0.214	0.269	0.116
First-order autocorrelation (AR_1)	0.425	0.432	0.477
Common interval	1950–2020	1950–2018	1950–2019
Variance of first principal component (PC1)	30.6%	56.4%	40.1%
Signal-to-noise ratio (S/N)	13.297	29.23	20.016
Expressed population signal (EPS)	0.93	0.967	0.952
First year of SSS > 0.85 (number of cores)	1916 (11)	1663 (7)	1541 (9)
Time span (CE)	1916–2014	1663–2014	1541–2014

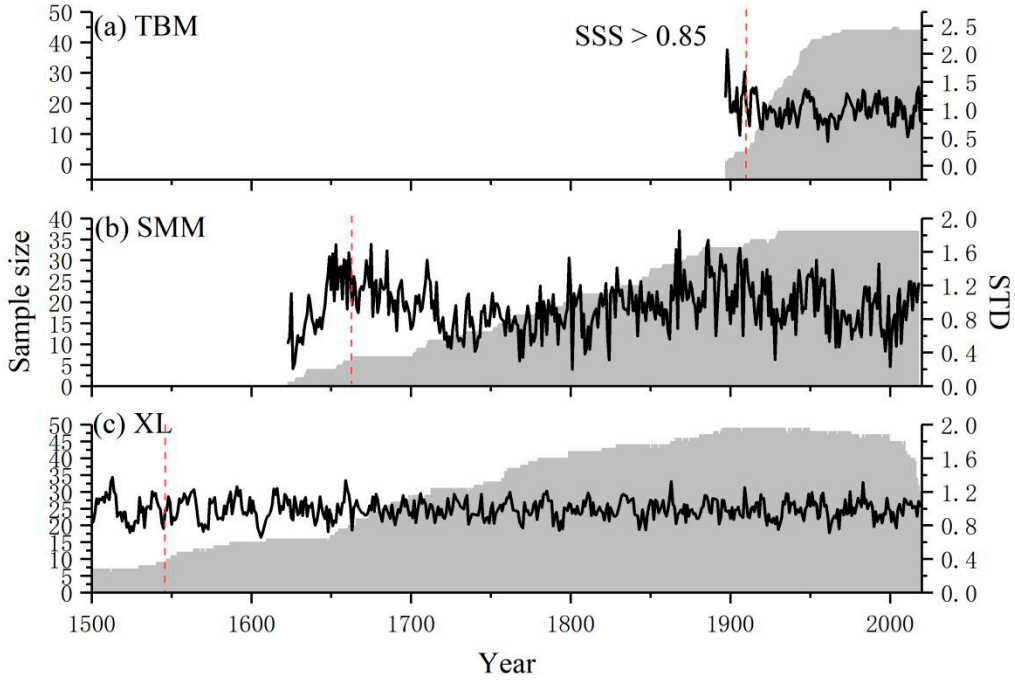

Figure 2. Chronology developed from TBM (**a**), SMM (**b**), and XL (**c**) and the corresponding SSS and sample size.

2.3. Climate Data and Data Analysis

The total precipitation, monthly mean temperature, and maximum and minimum temperature data were collected from meteorological stations located near the sample sites, namely, the Nanyang, Tianshui, and Ganzi stations. The data sources are depicted in Figure 1 and were accessed from the China Meteorological Administration website (http://data.cma.cn (accessed on 1 March 2020)). Meteorological data recording at Nanyang Station, Tianshui, and Ganzi commenced in 1954, 1953, and 1951, respectively. The self-calibrating Palmer Drought Severity Index (scPDSI) spanning the years 1850 to 2014 and with a resolution of 2.5° × 2.5° was employed as the drought criterion. The scPDSI data were obtained from the National Oceanic and Atmospheric Administration website (https://www.noaa.gov/ (accessed on 3 May 2022)).

The sea surface temperature (SST) dataset from the NOAA, Extended Reconstructed SST V5, was downloaded from https://www.noaa.gov/ (accessed on 3 May 2022). Long-term gridded mean maximum temperature and precipitation data (http://climexp.knmi.nl/start.cgi (accessed on 3 May 2022)), with 0.5° × 0.5° resolution, were obtained from CRU TS 4.05 [34], which was used to assess the spatial representation of the reconstructions and detect the forcing mechanisms, respectively.

Pearson's correlation coefficients were computed among the three chronologies to estimate the synchrony with each other, and it was also employed to investigate the relationship between the ring width index and climatic factors. Considering that tree growth is influenced by both the present growing season's conditions and the preceding year's conditions, Pearson's correlation coefficients were computed for the ring width index with monthly mean total precipitation, monthly mean temperature, and maximum and minimum temperatures, spanning from the previous September to the current August [35].

The split calibration–verification test method [36] was performed to verify the linear regression models [28]. This statistical analysis involved assessing various metrics, including correlation coefficient, explained variance, F-test value (F), sign test (ST), sign test of the first-order difference (ST1), reduction of error (RE), and coefficient of efficiency (CE) [35]. To ascertain the spatial–temporal representativeness of our reconstruction over a large region, spatial correlation analyses were conducted. Furthermore, the reliability of our reconstructions backward in time was assessed by comparing them with other warm-season mean maximum temperature reconstructions from nearby areas. Principal component analysis (PCA) was performed to extract common signals among chronologies in order to further detect the large-scale circulations' influence [37].

3. Results

3.1. Statistics of the Chronologies

As shown in Table 2, the mean sensitivity, a measure of relative difference in widths between adjacent rings, was 0.214 and 0.425 for TBM, 0.269 and 0.432 for SMM, and 0.116 and 0.477 for XL, respectively. The first-order autocorrelations were high, indicating that the tree-ring growth in our study sites is influenced by growth in the preceding year. Additionally, the signal-to-noise ratio (SNR) and the expressed population signal (EPS) for TBM were 13.297 and 0.93, respectively, while for SMM they were 29.23 and 0.967 and for XL they were 20.016 and 0.952. These statistical characteristics indicate that these chronologies have the potential to reflect past climates. Therefore, a 99- (1916–2014), 352- (1663–2014), and 474-year (1541–2014) chronology was developed for the TBM, SMM, and XL sites, respectively. These three chronologies do not agree well with each other, with a highest correlation of 0.3 and a lowest correlation of 0.1 during the common period 1916–2014 (Table 3). Further considering the location of the three sites and their environmental inhomogeneity in altitude, the single ring width index series was used to develop chronology.

Table 3. Annual correlation coefficients among the chronologies during the common period 1916–2014.

	TBM	**SMM**	**XL**
TBM	1		
SMM	0.10	1	
XL	0.16	0.30	1

3.2. Climate-Growth Response

The Pearson coefficients between different chronologies and four monthly climate variables, including precipitation, mean temperature, mean maximum, and mean minimum temperature, derived from the meteorological stations near the sample sites from September of the previous year to August of the current year are shown in Figure 3. In general, the ring width index derived from the TBM showed a relatively weak correlation with the four monthly climate variables from October to April (1954–2014). However, there was a significant positive correlation ($p < 0.05$) with total monthly precipitation in June. The ring width index and monthly mean, maximum, and minimum temperatures showed strong negative correlations between May and July, specifically for monthly mean and mean

maximum temperatures. These results indicate typical temperature stress on tree growth. We further evaluated the correlation between the ring width index and seasonally averaged climate factors. The strongest correlation (r = −0.56, $p < 0.01$) was observed between the ring width index and the mean maximum temperature from May to July from 1954 to 2014. At the SMM site (1953–2014), significantly positive correlations between the ring width index and precipitation were found from May to June. Additionally, significant anticorrelations between STD chronology and mean/maximum temperature were observed from May to July. However, the correlations between the ring width index and mean minimum temperature were weak, except in April. These findings suggest that moisture stress also influences tree growth during the growing season. We performed further computations to ascertain the relationship between the ring width index and the Self-Correcting Palmer Drought Severity Index (scPDSI) nearby. The scPDSI marks an enhancement over the original Palmer Drought Severity Index, which was introduced by Palmer in 1965 [38]. This advanced index is based on the equilibrium between water supply and demand, and it is calculated through a complex water-budget model that incorporates local soil characteristics alongside historical precipitation and potential evapotranspiration data [39,40]. The highest linear correlation (r = 0.42, $p < 0.01$) was observed between tree growth and early summer (May–July) scPDSI for the period 1953–2014, which further supports the hypothesis. In comparison, the temperature factor was more dominant in tree growth. Therefore, based on the analyses, the SMM chronology was used to reconstruct the May–July mean maximum temperature (r = −0.58, $p < 0.01$). As for the XL site, previous research averaged climatic data from the three meteorological stations during 1962–2019 to detect the climate–tree growth relationship and found that the most critical factor for growth is the May–June mean maximum temperature condition (r = 0.57, $p < 0.01$) [25]. This study found that the strongest correlation (0.57, $p < 0.01$) was between the ring width index and the May–July mean maximum temperature derived from Ganzi station for 1951–2014, one of the nearest meteorological stations. Therefore, to obtain a consistent signal and make comparisons with the other two sites mentioned above, the mean maximum temperatures of May–July were selected for reconstruction for further study.

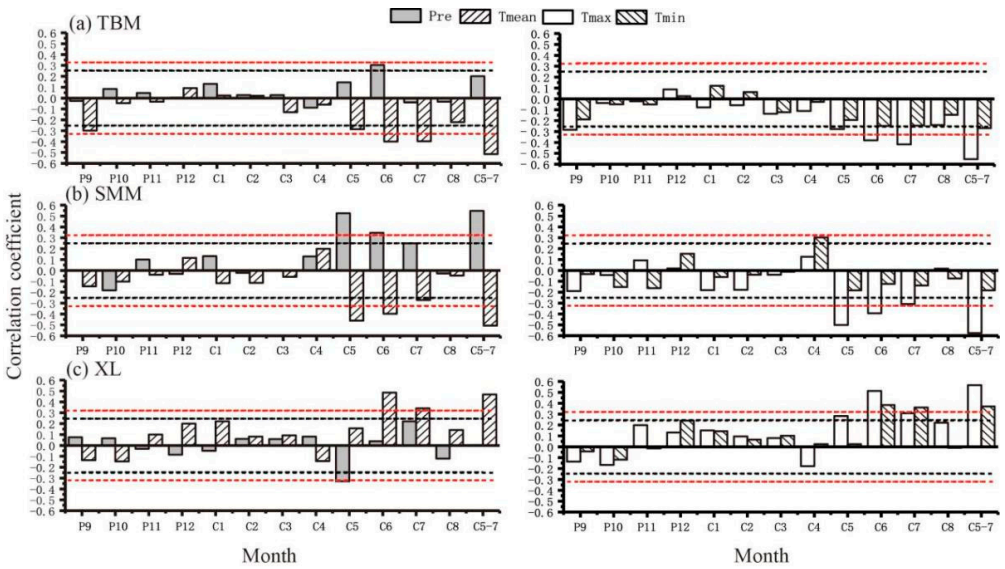

Figure 3. Correlations between STD of (**a**) TBM (1954–2014), (**b**) SMM (1953–2014), (**c**) XL (1951–2014), and monthly total precipitation, temperature, and monthly mean maximum and minimum temperature data from September to August, respectively. P and C indicate previous year and current year. The black and red dashed lines represent the corresponding 95% and 99% confidence levels, respectively.

3.3. May–July Mean Maximum Temperature Reconstructions

Based on the Pearson's correlation analyses discussed above, higher correlations were observed between tree ring indices and seasonalized mean maximum temperatures compared to correlations across individual months, indicating potential nonlinearity in climate–growth relationships in individual months [41]. Because the species of our study are evergreen, climate variables may have a continued effect on the growth of the trees [35, 42]. We further calculated the 31-year moving correlations between the three ring width indices and May–July mean maximum temperature. The results indicated that there were stable relationships specifically between tree growth and the seasonalized maximum temperature ($p < 0.05$). We thus consider that the linear reconstruction is able to recover the seasonalized maximum temperature, as has been shown in previous studies [43–46]. The linear regression models are designed as follows:

$$\text{(a) } T_{TBM5–7} = -2.705 \times STD_{TBM} + 32.525.$$

$$\text{(b) } T_{SMM5–7} = -2.2116 \times STD_{SMM} + 28.673.$$

$$\text{(c) } T_{XL5–7} = 4.1845 \times STD_{XL} + 15.794.$$

where $T_{TBM5–7}$, $T_{SMM5–7}$, and $T_{XL5–7}$ are the mean maximum temperatures from May to July, and STD_{TBM}, STD_{SMM}, and STD_{XL} represent the standard chronologies of TBM, SMM, and XL, respectively.

The results of the split-sample calibration-verification tests, which verify the fidelity of the models, are presented in Table 4. For models (a), (b), and (c), the values of r are statistically significant, and the values of RE are all positive, indicating rigorous model skill to some extent [47]. In comparison, the values of CE for model (b) and the latter half of the verification period for model (c) are lower. The values of ST1 for models (a) and (b) during the latter half of the verification period are not statistically significant, which may indicate that the reconstruction tracks the observation well in the low-frequency rather than the high-frequency domain. Nevertheless, the calibration and verification results for the entire period were ideal. The values of R were 0.56, 0.58, and 0.57, and the F values were 27.54, 29.67, and 29.1, respectively, exceeding the 99% confidence level, which indicates good model skill for reconstruction. In addition, the visual comparison shown in Figure 4 shows that the reconstruction tracked the actual mean maximum temperature values well. Based on the test and visual comparison results, we reconstructed the May–July mean maximum temperature changes at each site.

Table 4. Statistics of split calibration–verification test results for (a) TBM, (b) SMM, and (c) XL.

Model	Calibration					Verification					
	Period	r	R^2	$R^2_{aj.}$	F	Period	r	ST	ST1	RE	CE
(a)	1954–2014	0.56 **	0.31	0.3	27.54						
	1954–1984	0.69 **	0.48	0.46	26.86	1985–2014	0.43 **	21 *	18	0.11	0.11
	1985–2014	0.43 **	0.18	0.16	6.67	1954–1984	0.69 **	27 **	27 **	0.41	0.41
(b)	1953–2014	0.58 **	0.33	0.32	29.67						
	1953–1983	0.59 **	0.34	0.32	15.22	1984–2014	0.65 **	28 **	20	0.25	−0.01
	1984–2014	0.65 **	0.43	0.41	21.59	1953–1983	0.59 **	27 **	26 **	0.08	−0.6
(c)	1951–2014	0.57 **	0.32	0.31	29.1						
	1951–1982	0.58 **	0.34	0.32	15.44	1983–2014	0.6 **	27 **	25 **	0.25	−0.01
	1983–2014	0.6 **	0.36	0.34	16.77	1951–1982	0.58 **	26 **	24 **	0.26	0.02

Note: * and ** are the numbers of the same signs needed for 0.05 and 0.01 significance levels, respectively.

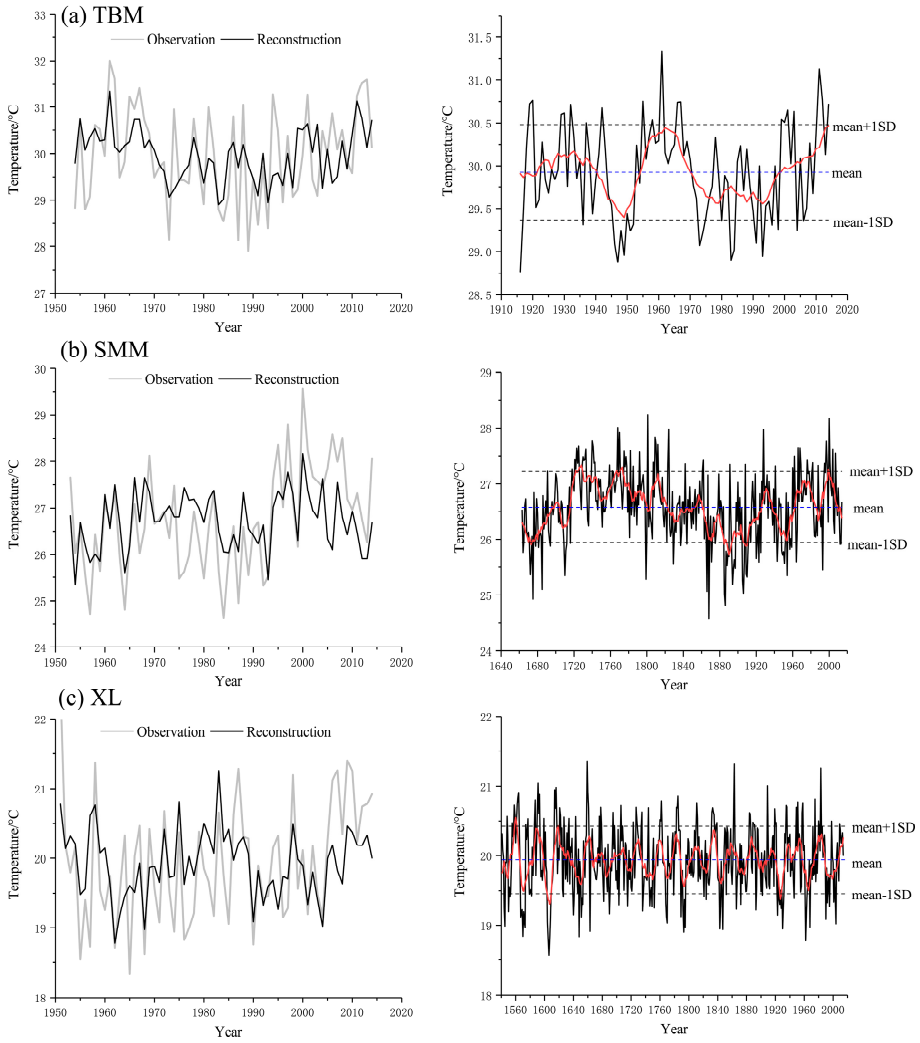

Figure 4. Comparison of reconstructed May–July maximum temperatures of (**a**) TBM, (**b**) SMM, and (**c**) XL with concurrent observed data, and characteristics of the reconstructed series. The data were smoothed with an 11-year running average and are shown in red.

3.4. Reconstructed Series Characteristics

In this study, our discussion primarily focused on inter-annual and inter-decadal temperature changes. The mean values of each reconstructed series present the normal status, with an extremely warm year identified as at least 1.5 SD above the mean and an extremely cold year at least 1.5 SD below the mean. To identify persistent warm or cold epochs, we applied an 11-year running average to each reconstruction (Figure 4; Table 5).

Table 5. Statistics of extremely warm and cold conditions and warm/cold epochs inferred from the reconstructions of (a) TBM, (b) SMM, and (c) XL.

Sites	Number of Warm Year	Number of Cold Year	Warm Epochs	Cold Epochs
TBM	4 (4%)	6 (6%)	1922–1940, 1955–1970, 1999–2014	1941–1954, 1971–1998
SMM	22 (6.3%)	26 (7.4%)	1717–1798, 1805–1817, 1963–1983, 1992–2007	1663–1695, 1705–1715, 1823–1852, 1861–1925, 1938–1962
XL	34 (7.2%)	34 (7.2%)	1552–1565, 1585–1598, 1612–1635, 1655–1666, 1696–1712, 1723–1734, 1735–1754, 1778–1788, 1803–1816, 1828–1839, 1852–1868, 1881–1896, 1943–1957, 1974–1988	1541–1551, 1566–1581, 1599–1611, 1639–1654, 1682–1692, 1765–1775, 1789–1802, 1817–1827, 1840–1851, 1869–1880, 1897–1908, 1921–1933, 1958–1973, 1989–2007

According to the TBM reconstruction, the mean of the reconstructed temperature was 29.93 °C and the SD was 0.55 °C. There were four warm summers (4% of the total) and six cold summers (6% of the total). Additionally, three persistent warm epochs, including 1922–1940, 1955–1970, 1999–2014, and two persistent cold epochs, including 1941–1954 and 1971–1998, were found over the past 99 years. For SMM reconstruction, the mean reconstructed temperature was 26.58 °C and the SD was 0.63 °C. A total of 22 warm summers (6.3% of the total) and 26 cold summers (7.4% of the total) were observed. Four persistent warm epochs and five persistent cold epochs were observed over the past 352 years. According to the XL reconstruction, the mean reconstructed temperature was 19.94 °C and the SD was 0.48 °C. Over the past 474 years, 34 warm summers (7.2% of the total), 34 cold summers (7.2% of the total), 14 persistent warm epochs, and 14 persistent cold epochs were observed. In addition, during the past 60 years, the reconstructed mean maximum temperature was higher than the mean.

The spectral power of the reconstructions was examined using MTM. As shown in Figure 5, significant peaks ($p < 0.05$) were found at 2.6–2.8, 2.1–3.1, and 2.3–5.7 years in TBM, SMM, and XL reconstructions, respectively, which fall within the cycle of the El Niño–Southern Oscillations (ENSO) [47,48]. Additionally, significant peaks found at 24–35 and 34–40 years in SMM and XL records may indicate connections at lower frequencies of regional temperature with the Pacific Decadal Oscillation (PDO) [33] and Atlantic Multidecadal Oscillation (AMO) [49,50], respectively. These results indicate that ENSO is a common signal that influences the May–July mean maximum temperature change over mid-latitude China. The details of this are discussed in the following sections.

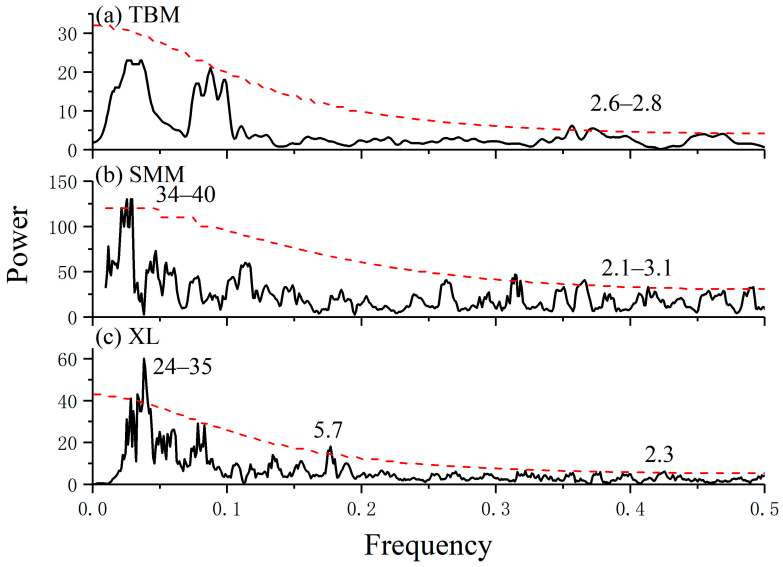

Figure 5. Multi-taper method analysis of reconstructed temperature series of (**a**) TBM, (**b**) SMM, and (**c**) XL. The dotted line denotes a 95% significance level.

4. Discussion and Conclusions

4.1. Climate–Radial Tree Growth Relationships

Confirmation of the climate–tree growth relationships at these three sample sites revealed that tree growth is primarily influenced by the concurrent mean maximum temperature during the period from May to July.

At the Nanyang meteorological station, the multi-year mean annual total precipitation exceeded 790 mm from 1954 to 2019. The abundance of precipitation during the growing season adequately fulfills the growth requirements of *Pinus massoniana* trees in east–central

China. Consequently, this leads to an insignificant correlation between the tree-ring width index and precipitation for most of the months in the TBM.

Usually, *Pinus tabulaeformis* trees are found in regions with an annual total precipitation exceeding 500 mm [51]. However, as recorded by the Tianshui meteorological station, the multi-year mean annual total precipitation was 515 mm from 1953 to 2019, which just meets the need for *Pinus tabulaeformis* tree growth in north–central China. Physiological studies have shown that during the early growing season, xylogenesis is triggered by increased precipitation, provided that temperature conditions are suitable [52]. As a result, significantly positive correlations were observed between TBM and June precipitation and SMM and precipitation from May to June. However, notable negative correlations between the ring width index inferred from TBM and SMM and the mean and maximum temperatures from May to July suggested that the elevated temperatures in these three months could potentially slow down tree growth. During the early growing season, elevated temperatures, particularly the mean maximum temperature, can intensify water stress through increased evaporation and evapotranspiration, leading to decreased soil moisture levels. When moisture falls below the threshold conducive to tree growth, the stomata close as a response. Consequently, the reduced photosynthetic efficiency results in diminished radial growth [52]. These inferences are also supported by the correlation analysis results of the tree-ring width index and local moisture conditions (scPDSI). Considering XL, the sample site is located at 3880 m a.s.l. Due to the higher altitude, the temperature is low enough to limit tree growth. Therefore, tree growth in this forest zone usually has high positive correlations with mean, maximum, and minimum temperatures. Additionally, in the semi-humid area of the TP, early summer is a vigorous period of tree growth. Higher temperatures are beneficial for photosynthesis and cambium cell division, as well as the formation of wider rings [24]. Therefore, the radial growth of *Picea balfouriana* in the southeastern TP was significantly positively correlated with the maximum May–July temperature. In general, the radial growth in these three sites is significantly correlated with the maximum May–July temperature, which has a clear physiological significance.

4.2. Spatial–Temporal Representativeness of the Reconstructions

The spatial correlation between each of our reconstructions and concurrent actual gridded mean maximum temperature data is shown in Figure 6. These results reveal that each of the reconstructed mean maximum temperatures is representative of the May–July mean maximum temperature change at the regional scale. Furthermore, these correlation patterns exhibit similarities to those derived from the actual gridded maximum temperature data obtained from meteorological station records. This similarity indicates that our reconstructions are reliable for assessing large-scale changes in the May–July mean maximum temperature.

To further detect whether our reconstructions are reliable backward in time, we compared the reconstructions with other warm-season temperature reconstructions from nearby regions. As shown in Figure 7, the pronounced warm epochs in the 1920s–1930s and 1960s and the persistent cold epoch in the 1950s and 1980s, inferred from the TBM, are in accord with the maximum temperature inferred from the tree-ring data in the Funiu Mountains and eastern Qinling Mountains in central China [17]. Additionally, two pronounced warm epochs in 1922–1940 and 1999–2014 and two cold epochs in 1941–1954 and 1971–1998, recorded in TBM, were also found in the January-July minimum temperature reconstruction in the Dabie Mountains [44]. As for the SMM reconstruction, two warm epochs were recorded in the 1760s–1770s and 1990s–2000s, and three cold epochs in the 1660s–1670s, 1870s–1920s, and 1940s–1950s presented one-to-one correspondence with the May–June mean maximum temperature reconstruction based on the mean early wood density derived

from the same region [53]. The continuous cold period from 1861 to 1925 and the warm period from 1902 to 2007 were also reflected by the reconstructed March-October mean maximum temperature variations inferred from *Picea purpurea* in Gansu Province. Additionally, the reconstructed variations in the SMM were well accordant with the temperature reconstruction in the Kongtong Mountains, including two pronounced warm epochs in 1805–1817 and 1902–2007 and two cold epochs in 1851–1925 and 1938–1962. As for the XL reconstruction, three warm epochs in 1655–1666, 1723–1734, and 1852–1868 and three cold epochs in 1765–1775, 1817–1827, and 1869–1880 from the XL reconstruction were also identified in July–August mean maximum temperature reconstruction in the northwestern Sichuan Plateau [9]. What is more, the reliability of the reconstruction based on XL data has been confirmed by Zhang et al. [25]. It is worth noting that there are some differences when comparing our reconstructions with other reconstructions nearby, and these differences may occur because of the deviations caused by the use of different detrending methods, reconstruction time periods, and reconstruction objects. However, the correlation coefficient of our reconstructions with others nearby is high at decadal timescales (r = 0.38 and r = 0.46). Therefore, our reconstructions are representative of the large-scale May–July mean maximum temperature changes in each region over mid-latitude China during the reconstructed periods.

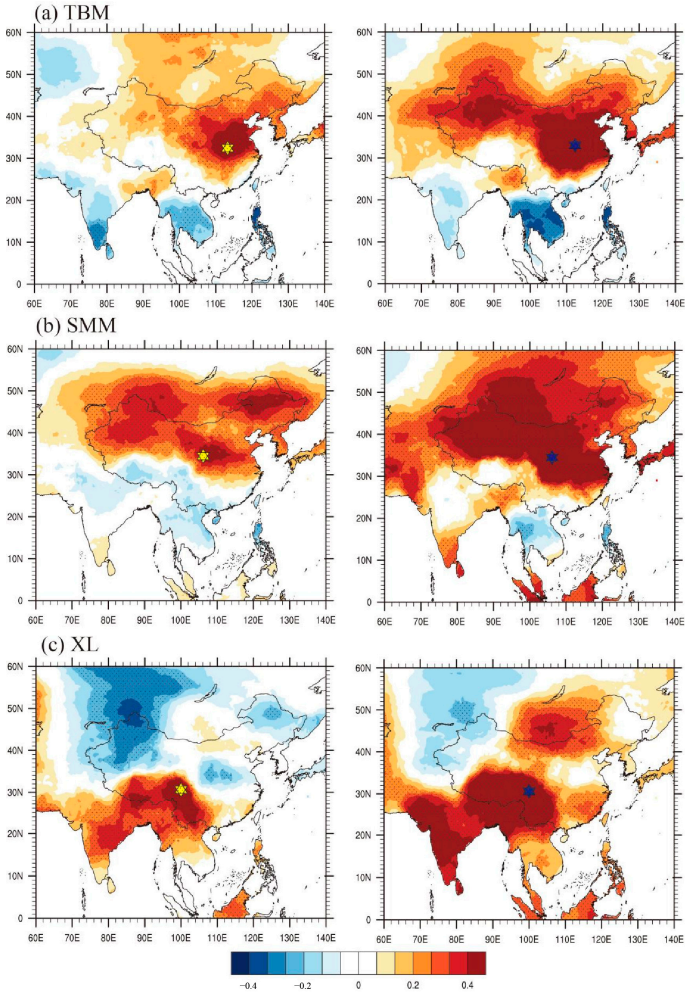

Figure 6. Spatial correlation between reconstructed May–July mean maximum temperature of (**a**) TBM, (**b**) SMM, (**c**) XL, and observed gridded data (**left**) and May–July mean maximum temperature recorded at meteorological stations and actual gridded data (**right**). The red and blue stars denote the locations of sample sites and the corresponding meteorological stations.

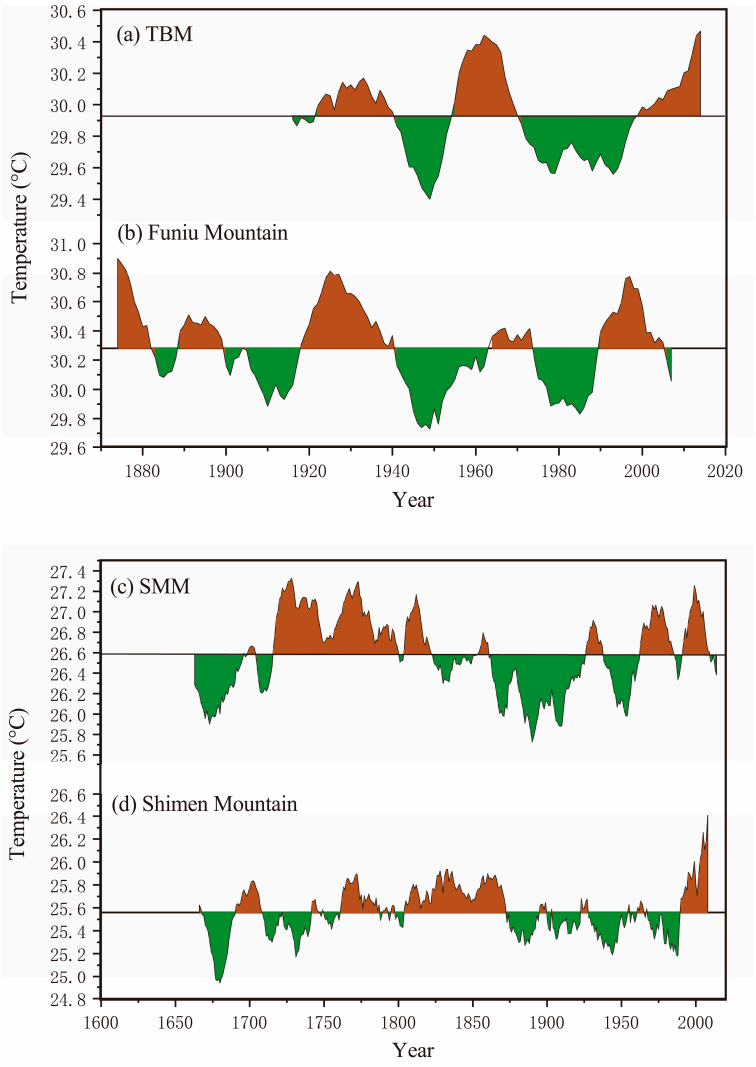

Figure 7. Comparison of the reconstructed mean maximum May–July temperature with other tree-ring-based temperature reconstructions near our study area. (**a**) The reconstructed mean maximum May–July temperature from TBM in the study; (**b**) the mean maximum May–July temperature reconstruction inferred from Funiu Mountain in the eastern Qinling Mountains [17]; (**c**) the reconstructed mean maximum May–July temperature from SMM in the study; (**d**) the mean maximum May–July temperature reconstruction inferred from Shimen Mountain in the transition zone between the Loess Plateau and the Qinling Mountains [53]. Here, an 11-year running average was performed for all series and the correlated coefficients were calculated based on the running average. The orange and green shades indicate the warm and cold periods, respectively.

4.3. Possible Factors Influencing Tree-Ring-Based Temperature Reconstruction and Comparison

As discussed above, all three temperature reconstructions have spatial–temporal representativeness at regional scales. However, inconsistent changes can be observed during common periods in instrumental observations and reconstructions. As shown in Figure 8a, the 11-year running correlation coefficients among the May–July mean maximum temperature inferred from these three tree-ring indices fluctuated during the common period 1916–2014. Specifically, in the 1920s, 1960s, and 2000s, the correlation among the three reconstructions was much weaker, which indicated that the May–July mean maximum temperature change over mid-latitude China was inconsistent. For example, cold epochs were observed in the 1950s inferred from TBM and SMM. The mean maximum temperature, also inferred from XL, also experienced a cold epoch at the end of the 1950s (Table 5). These common cold epochs were also recorded in other temperature reconstructions across

mid-latitude China [22,27]. However, around the 1960s, the three reconstructions show different epochs. The temperature changes inferred from TBM and SMM were warm, while those from XL were cold. Furthermore, the relationships between SMM and XL reconstructions were calculated and the correlation coefficients fluctuated from 1668 to 2009 (Figure 8b). The results indicated that inconsistent changes in May–July mean maximum temperature inferred from tree-ring data over mid-latitude China remained at longer timescales. Additionally, it is worth noting that in recent decades, the three reconstructions experienced a different warming trend against the background of global warming. An ensuing question is what would be responsible for the inconsistencies in tree-ring-based temperature reconstructions during comparisons over mid-latitude China.

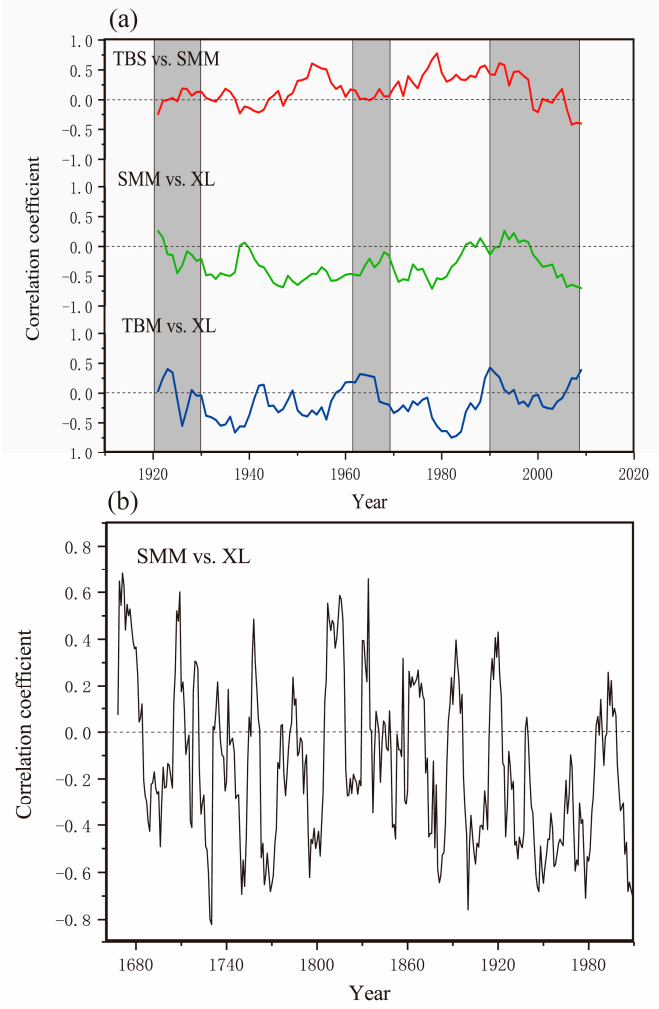

Figure 8. An 11-year running correlation among the reconstructions. (**a**) The correlation coefficients among the reconstructions for 1916–2014; (**b**) the correlation coefficients between SMM and XL for 1668–2009. The gray rectangles indicate the weak correlation periods among the reconstructions.

Except for the fact that the reconstructions cannot explain all the observed mean maximum temperature variances, one possibility is the regional differences in the May–July mean maximum temperature change. Firstly, the Mann–Kendall trend test was used to analyze the changes in the May–July maximum temperature recorded by the three meteorological stations. As shown in Table 6, the Z-values of the variation trend of the May–July mean maximum temperature recorded at the Nanyang meteorological station (1953–2014), the Tianshui meteorological station (1953–2014), and the Ganzi meteorological station (1951–2014) were 0.06, 3.16, and 2.51, respectively. These indicate that the May–July maximum temperatures recorded at the Tianshui and Ganzi stations showed

an obvious warming trend. In addition, there was no significant change trend in the concurrent precipitation recorded at the three meteorological stations. Therefore, given the regional differences in the May–July maximum temperature over mid-latitude China, the reconstructions have shown different trends in recent decades.

Table 6. The results of the Mann–Kendall trend test for climatic factors recorded at three meteorological stations.

Climatic Factors	Station	Z Value	*p*
May–July mean maximum temperature/ May–July precipitation	Nanyang	0.06/0.56	0.952/0.576
	Tianshui	3.16/1.14	0.002 **/0.256
	Ganzi	2.51/1.01	0.012 */0.311
May–July precipitation	Nanyang	0.56	0.576
	Tianshui	1.14	0.256
	Ganzi	1.01	0.311

Note: * and ** are the numbers of the same signs needed for 0.05 and 0.01 significance levels, respectively.

Another possibility is the influence of different precipitation signals on the mean maximum temperature. As shown in Figure 3, the SMM chronology showed a significantly positive correlation with precipitation from May to July, suggesting that there is a different precipitation signal compared to the TBM and XL chronologies. Additionally, the results of the partial correlation analysis demonstrate that (Figure 9) when controlling for the effect of May–July mean maximum temperature, both the TBM and XL chronologies have no significant partial correlations with monthly precipitation from the prior September to the current August, whereas the partial correlations for the SMM chronology are higher and significant in June. The results suggest that the SMM chronology records strong precipitation signals, whereas the TBM and XL contain relatively little precipitation information compared to the SMM chronology. As a result, the positive precipitation information and negative temperature signals recorded in SMM may influence or interfere with each other in terms of their respective trends [54]. Therefore, to some extent, the SMM reconstruction may imperfectly estimate extreme warm/cold epochs, leading to discrepancies in the reconstructed May–July mean maximum temperatures compared to other reconstructions.

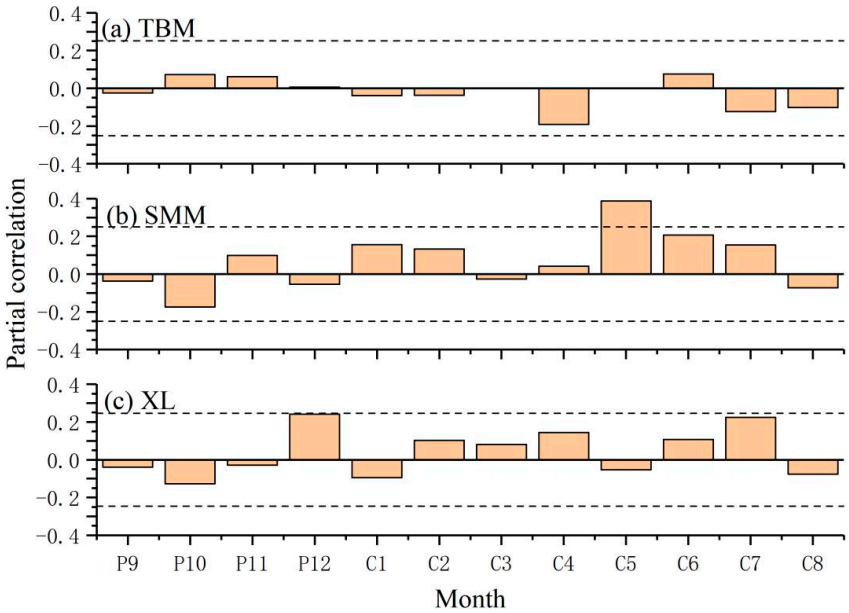

Figure 9. Partial correlations between the STD of (**a**) TBM (1954–2014), (**b**) SMM (1953–2014), (**c**) XL (1951–2014), and monthly precipitation when the effect of May–July mean maximum temperature is controlled.

The third possibility is ENSO. The results of the spectral power analysis showed significant peaks at approximately 2–5 years in our reconstructions, which fall within the overall bandwidth of ENSO. To investigate the spatial pattern of the May–July mean maximum temperature and explore its possible association with ENSO, the principal component analysis method was used to extract temperature signals from the three reconstructions. The eigenvalue of the first principal component (PC1) is 1.39, the cumulative variance contribution is 46%, and the load of the three chronologies on PC1 is positive, indicating that PC1 captures most of the variability in each chronology. The spatial correlation between PC1 and the actual mean maximum temperature data was further calculated (Figure 10), showing a significant positive correlation with the temperatures in the XL region and a significant negative correlation with the temperatures in the TBM and SMM regions. This emphasizes the spatial variability in the May–July mean maximum temperatures across mid-latitude China.

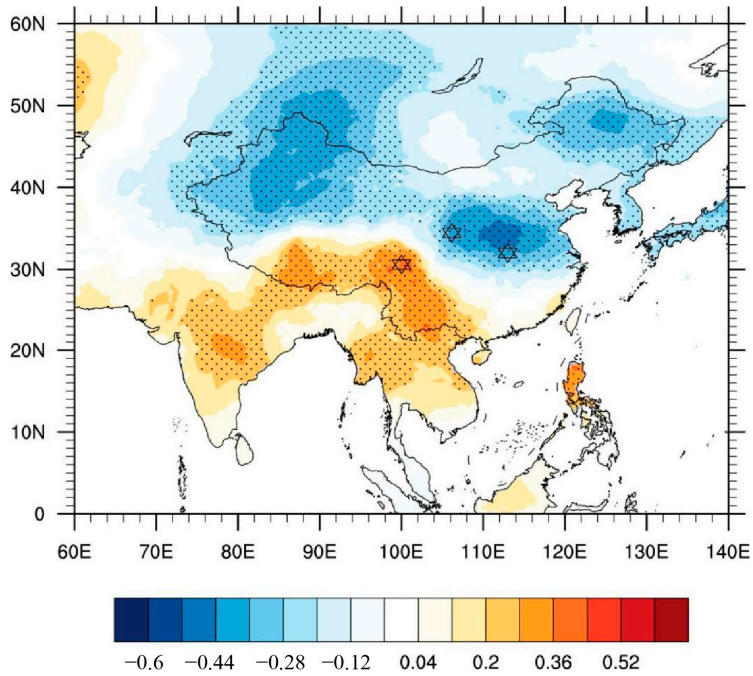

Figure 10. Spatial correlation between PC1 and observed May–July mean maximum temperature (1951–2014). The black stars and dots denote the locations of sample sites and that the correlation coefficient passes 90% confidence level test.

Additionally, the temporal variation of PC1 exhibits distinct inter-annual variation, which is closely linked to the Niño 3.4 SST. This notion is further supported by the results correlating PC1 and SST over the global ocean, which exhibits a typical SST pattern associated with El Niño (Figure 11). The results suggest that when the eastern tropical Pacific is warm (El Niño condition), the May–July mean maximum temperature over the area nearby XL increases, whereas that over the area near TBM and SMM would decrease and vice versa when the eastern tropical Pacific is cold (La Niña condition) [55]. What is more, both the PDO and AMO modulate the relationship between ENSO and temperature change in China [56,57], which further confirms the interdecadal cycles inferred from our reconstructions.

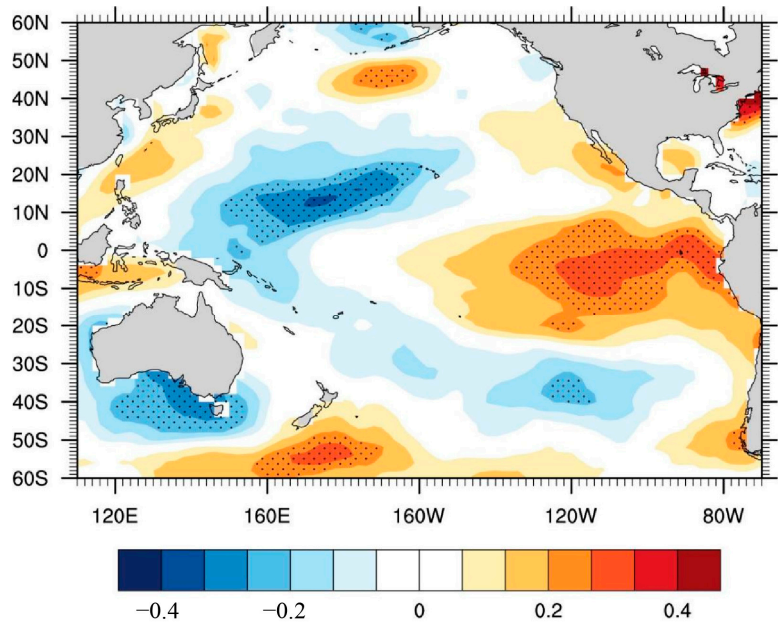

Figure 11. Spatial correlation between PC1 and SST (1951–2014). The black dots denote that the correlation coefficient passes 90% confidence level test.

5. Conclusions

In this study, we presented three tree-ring width chronologies over mid-latitude China. Upon analyzing the correlations among the STD chronologies and their correlation coefficients with various climatic factors recorded at the nearby meteorological stations, we found that the May–July mean maximum temperature was the controlling factor for the tree growth in our sampling sites. Then, we proceeded to reconstruct the May–July mean maximum temperature variations using linear regression models. Spatial correlation analysis of our reconstructions with concurrent observed data, as well as a comparison of our reconstructions with other nearby reconstructions, confirmed the large-scale representativeness of our reconstructions backwards in time. However, our reconstructions show an inconsistent change in the May–July mean maximum temperature during the common periods 1916–2014 during comparisons. Therefore, possible forcing factors for these discrepancies were further detected. Regional differences in responding to global warming, the influence of different precipitation signals on the maximum temperature, and ENSO are attributed to the discrepancies of the May–July maximum temperature change in instrumental observations and proxy data over mid-latitude China. In the context of global climate change, this study provides a reference for regional discrepancies in mean maximum temperature variation in past centuries over mid-latitude China. However, some uncertainties might affect our results. First, total ring width was employed to track long-term temperature variations. In some cases, other tree-ring parameters, such as density or stable carbon isotope in tree-ring cellulose may provide a stronger temperature signal, which may much better reveal the discrepancies in the May–July mean maximum temperature over mid-latitude China [53,58,59]. Therefore, in future studies, more tree-ring parameters should be applied. Second, our discussion on the possible factors for the regional May–July mean maximum temperature discrepancies was based on the instrumental observations and the influence of ENSO, considering inter-annual variation. However, the influence of PDO and AMO, which are inter-decadal variations, would also affect temperature change over mid-latitude China. Therefore, longer chronologies and modeling experiments are required.

Author Contributions: Z.Z. and Z.W. conceived this study and wrote the manuscript; Y.Z. provided suggestions to improve them. All authors have read and agreed to the published version of the manuscript.

Funding: This research was funded by the Second Tibetan Plateau Scientific Expedition and Research (STEP) program (no. 2019QZKK0608), the Natural Science Foundation of Sichuan Province (No. 2022NSFSC0215), and the Natural Science Foundation of China (No. 42201010).

Institutional Review Board Statement: Not applicable.

Informed Consent Statement: Not applicable.

Data Availability Statement: The data of this study are available upon request to the first author or the corresponding author due to privacy.

Acknowledgments: Z.Z. and W.Z. are thankful to Xiaohua Gou and other students in the Tree-ring Laboratory, College of Earth and Environmental Sciences, Lanzhou University for the necessary facilities and constant support.

Conflicts of Interest: On behalf of all authors, the corresponding author states that there are no conflicts of interest.

References

1. AR6 Synthesis Report: Climate Change 2023—IPCC. Available online: https://www.ipcc.ch/report/sixth-assessment-report-cycle/ (accessed on 24 November 2024).
2. Panin, G.N.; Solomonova, I.V.; Vyruchalkina, T.Y. Climatic Trends in the Middle and High Latitudes of the Northern Hemisphere. *Water Resour.* **2009**, *36*, 718–730. [CrossRef]
3. Jones, P.D.; Briffa, K.R. Global Surface Air Temperature Variations During the Twentieth Century: Part 1, Spatial, Temporal and Seasonal Details. *Holocene* **1992**, *2*, 165–179. [CrossRef]
4. Yao, T.; Xue, Y.; Chen, D.; Chen, F.; Thompson, L.; Cui, P.; Koike, T.; Lau, W.K.-M.; Lettenmaier, D.; Mosbrugger, V. Recent Third Pole's Rapid Warming Accompanies Cryospheric Melt and Water Cycle Intensification and Interactions between Monsoon and Environment: Multidisciplinary Approach with Observations, Modeling, and Analysis. *Bull. Am. Meteorol. Soc.* **2019**, *100*, 423–444. [CrossRef]
5. Karl, T.R.; Kukla, G.; Razuvayev, V.N.; Changery, M.J.; Quayle, R.G.; Heim, R.R., Jr.; Easterling, D.R.; Fu, C.B. Global Warming: Evidence for Asymmetric Diurnal Temperature Change. *Geophys. Res. Lett.* **1991**, *18*, 2253–2256. [CrossRef]
6. Meehl, G.A.; Tebaldi, C. More Intense, More Frequent, and Longer Lasting Heat Waves in the 21st Century. *Science* **2004**, *305*, 994–997. [CrossRef] [PubMed]
7. Photiadou, C.; Jones, M.R.; Keellings, D.; Dewes, C.F. Modeling European Hot Spells Using Extreme Value Analysis. *Clim. Res.* **2014**, *58*, 193–207. [CrossRef]
8. Wang, W.; Zhou, W.; Li, Y.; Wang, X.; Wang, D. Statistical Modeling and CMIP5 Simulations of Hot Spell Changes in China. *Clim. Dyn.* **2015**, *44*, 2859–2872. [CrossRef]
9. Zhu, L.; Zhang, Y.; Li, Z.; Guo, B.; Wang, X. A 368-Year Maximum Temperature Reconstruction Based on Tree-Ring Data in the Northwestern Sichuan Plateau (NWSP), China. *Clim. Past* **2016**, *12*, 1485–1498. [CrossRef]
10. Shi, Y.; Fan, J. Glimatic Warming and Drying Trend and Its Impact on Water Resources in Mid Latitude China. *Adv. Water Sci.* **1991**, *2*, 217–223.
11. Douville, H.; Colin, J.; Krug, E.; Cattiaux, J.; Thao, S. Midlatitude Daily Summer Temperatures Reshaped by Soil Moisture under Climate Change. *Geophys. Res. Lett.* **2016**, *43*, 812–818. [CrossRef]
12. Yang, Q.; Ma, Z.; Xu, B. Modulation of Monthly Precipitation Patterns over East China by the Pacific Decadal Oscillation. *Clim. Change* **2017**, *144*, 405–417. [CrossRef]
13. Yang, Q.; Ma, Z.; Wu, P.; Klingaman, N.P.; Zhang, L. Interdecadal Seesaw of Precipitation Variability between North China and the Southwest United States. *J. Clim.* **2019**, *32*, 2951–2968. [CrossRef]
14. Wilson, R.J.S.; Luckman, B.H. Tree-Ring Reconstruction of Maximum and Minimum Temperatures and the Diurnal Temperature Range in British Columbia, Canada. *Dendrochronologia* **2002**, *20*, 257–268. [CrossRef]
15. Liu, Y.; Wang, Y.; Li, Q.; Sun, J.; Song, H.; Cai, Q.; Zhang, Y.; Yuan, Z.; Wang, Z. Reconstructed May–July Mean Maximum Temperature since 1745AD Based on Tree-Ring Width of Pinus Tabulaeformis in Qianshan Mountain, China. *Palaeogeogr. Palaeoclimatol. Palaeoecol.* **2013**, *388*, 145–152. [CrossRef]
16. Sun, Y.; Wang, L.; Chen, J.; Duan, J. Reconstructing Mean Maximum Temperatures of May–August from Tree-Ring Maximum Density in North Da Hinggan Mountains, China. *Chin. Sci. Bull.* **2012**, *57*, 2007–2014. [CrossRef]

17. Tian, Q.; Liu, Y.; Cai, Q.; Bao, G.; Wang, W.; Xue, W.; Zhu, W.; Song, H.; Lei, Y. The maximum temperature of May–July inferred from tree-ring in Funiu Mountain since 1874 AD. *Acta Geogr. Sin.* **2009**, *64*, 879–887. [CrossRef]
18. Chen, J.; Wang, L.; Zhu, H.; Wu, P. Reconstructing Mean Maximum Temperature of Growing Season from the Maximum Density of the Schrenk Spruce in Yili, Xinjiang, China. *Chin. Sci. Bull.* **2009**, *54*, 2300–2308. [CrossRef]
19. Duan, J.; Zhang, Q.-B.; Lv, L.; Zhang, C. Regional-Scale Winter-Spring Temperature Variability and Chilling Damage Dynamics over the Past Two Centuries in Southeastern China. *Clim. Dyn.* **2012**, *39*, 919–928. [CrossRef]
20. Li, J.; Shao, X.; Li, Y.; Qin, N.; Yang, T. The Relationship between Early Summer Air Temperature and the Global Sea Surface Temperature in the North of Western Sichuan Plateau from 1854 to 2010. *J. Desert Res.* **2015**, *35*, 1024–1035.
21. Keyimu, M.; Li, Z.; Liu, G.; Fu, B.; Fan, Z.; Wang, X.; Wu, X.; Zhang, Y.; Halik, U. Tree-Ring Based Minimum Temperature Reconstruction on the Southeastern Tibetan Plateau. *Quat. Sci. Rev.* **2021**, *251*, 106712. [CrossRef]
22. Liu, Y.U.; Linderholm, H.W.; Song, H.; Cai, Q.; Tian, Q.; Sun, J.; Chen, D.; Simelton, E.; Seftigen, K.; Tian, H.U.A. Temperature Variations Recorded in Pinus Tabulaeformis Tree Rings from the Southern and Northern Slopes of the Central Qinling Mountains, Central China. *Boreas* **2009**, *38*, 285–291. [CrossRef]
23. Tian, Q.; Helama, S.; Zhao, P. Temperature Variability Inferred from Tree Rings of Qinling Region in North-Central China. In Proceedings of the 2011 International Symposium on Water Resource and Environmental Protection, Xi'an, China, 20–22 May 2011; IEEE: Piscataway, NJ, USA, 2011; pp. 2072–2075.
24. Zheng, Z.; Jin, L.; Li, J.; Chen, J.; Zhang, X.; Wang, Z. Moisture Variation Inferred from Tree Rings in North Central China and Its Links with the Remote Oceans. *Sci. Rep.* **2021**, *11*, 16463. [CrossRef] [PubMed]
25. Zhang, Y.; Li, J.; Zheng, Z.; Zeng, S. A 479-Year Early Summer Temperature Reconstruction Based on Tree-Ring in the Southeastern Tibetan Plateau, China. *Atmosphere* **2021**, *12*, 1251. [CrossRef]
26. Liu, Y.; Qin, Y.; Ge, Q.; Dai, J.; Chen, Q. Reponses and Sensitivities of Maize Phenology to Climate Change from 1981 to 2009 in Henan Province, China. *J. Geogr. Sci.* **2017**, *27*, 1072–1084. [CrossRef]
27. Song, H.; Liu, Y.; Li, Q.; Gao, N.; Ma, Y.; Zhang, Y. Tree-Ring Based May–July Temperature Reconstruction since AD 1630 on the Western Loess Plateau, China. *PLoS ONE* **2014**, *9*, e93504. [CrossRef] [PubMed]
28. Cook, E.R.; Kairiukstis, L.A. *Methods of Dendrochronology: Applications in the Environmental Sciences*; Springer Science & Business Media: Berlin, Germany, 2013; ISBN 978-94-015-7879-0.
29. Stokes, M.A. *An Introduction to Tree-Ring Dating*; University of Arizona Press: Tucson, AZ, USA, 1996; ISBN 978-0-8165-1680-3.
30. Holmes, R.L. Computer-Assisted Quality Control in Tree-Ring Dating and Measurement. *Tree Ring Bull.* **1983**, *43*, 51–67.
31. Cook, E.R. A Time Series Analysis Approach to Tree Ring Standardization (Dendrochronology, Forestry, Dendroclimatology, Autoregressive Process). Ph.D. Thesis, The University of Arizona, Tucson, AZ, USA, 1985.
32. Zheng, Z.; Jin, L.; Li, J.; Chen, J.; Zhang, X.; Wang, Z. Influence of May–June Frontal Precipitation on Coherent Moisture Pattern in East-Central China since 1793 Based on Tree-Ring Data. *Quat. Int.* **2022**, *607*, 79–88. [CrossRef]
33. Wigley, T.M.; Briffa, K.R.; Jones, P.D. On the Average Value of Correlated Time Series, with Applications in Dendroclimatology and Hydrometeorology. *J. Appl. Meteorol. Climatol.* **1984**, *23*, 201–213. [CrossRef]
34. Version 4 of the CRU TS Monthly High-Resolution Gridded Multivariate Climate Dataset | Scientific Data. Available online: https://www.nature.com/articles/s41597-020-0453-3 (accessed on 26 July 2023).
35. Fritts, H. *Tree Rings and Climate*; Elsevier: Amsterdam, The Netherlands, 2012; ISBN 978-0-323-14528-2.
36. Meko, D.; Graybill, D.A. Tree-Ring reconstruction of upper gila rwer discharge. *JAWRA J. Am. Water Resour. Assoc.* **1995**, *31*, 605–616. [CrossRef]
37. Jolliffe, I.T. Principal Component Analysis: A Beginner's Guide—I. Introduction and Application. *Weather* **1990**, *45*, 375–382. [CrossRef]
38. Palmer, W.C. *Meteorological Drought*; U.S. Department of Commerce, Weather Bureau: Silver Spring, MD, USA, 1965.
39. Li, J.; Cook, E.R.; D'arrigo, R.; Chen, F.; Gou, X. Moisture Variability across China and Mongolia: 1951–2005. *Clim. Dyn.* **2009**, *32*, 1173–1186. [CrossRef]
40. Van Der Schrier, G.; Barichivich, J.; Briffa, K.R.; Jones, P.D. A scPDSI-based Global Data Set of Dry and Wet Spells for 1901–2009. *JGR Atmos.* **2013**, *118*, 4025–4048. [CrossRef]
41. Fang, K.; Gou, X.; Chen, F.; Frank, D.; Liu, C.; Li, J.; Kazmer, M. Precipitation Variability during the Past 400 Years in the Xiaolong Mountain (Central China) Inferred from Tree Rings. *Clim. Dyn.* **2012**, *39*, 1697–1707. [CrossRef]
42. Zheng, Y.; Zhang, Y.; Shao, X.; Yin, Z.-Y.; Zhang, J. Temperature Variability Inferred from Tree-Ring Widths in the Dabie Mountains of Subtropical Central China. *Trees* **2012**, *26*, 1887–1894. [CrossRef]
43. Shi, C.; Masson-Delmotte, V.; Daux, V.; Li, Z.; Zhang, Q.-B. An Unstable Tree-Growth Response to Climate in Two 500 Year Chronologies, North Eastern Qinghai-Tibetan Plateau. *Dendrochronologia* **2010**, *28*, 225–237. [CrossRef]
44. Shi, J.; Cook, E.R.; Li, J.; Lu, H. Unprecedented January–July Warming Recorded in a 178-Year Tree-Ring Width Chronology in the Dabie Mountains, Southeastern China. *Palaeogeogr. Palaeoclimatol. Palaeoecol.* **2013**, *381–382*, 92–97. [CrossRef]

45. Liu, Y.; Zhang, Y.; Song, H.; Ma, Y.; Cai, Q.; Wang, Y. Tree-Ring Reconstruction of Seasonal Mean Minimum Temperature at Mt. Yaoshan, China, since 1873 and Its Relevance to 20th-Century Warming. *Clim. Past Discuss.* **2014**, *10*, 859–894.
46. Li, J.; Jin, L.; Zheng, Z. A 278-Year Summer Minimum Temperature Reconstruction Based on Tree-Ring Data in the Upper Reaches of Dadu River. *Forests* **2023**, *14*, 832. [CrossRef]
47. Fang, K.; Gou, X.; Chen, F.; D'Arrigo, R.; Li, J. Tree-Ring Based Drought Reconstruction for the Guiqing Mountain (China): Linkages to the Indian and Pacific Oceans. *Int. J. Climatol.* **2010**, *30*, 1137–1145. [CrossRef]
48. Allan, R.; Lindesay, J.; Parker, D. *El Nino Southern Oscillation and Climate Variability*; CSIRO Publishing: Clayton, Australia, 1996.
49. Multi-Scale Dynamical Analysis (MSDA) of Sea Level Records Versus PDO, AMO, and NAO Indexes | Climate Dynamics. Available online: https://link.springer.com/article/10.1007/s00382-013-1771-3#citeas (accessed on 1 December 2024).
50. Le Goff, H.; Flannigan, M.D.; Bergeron, Y.; Girardin, M.P. Historical Fire Regime Shifts Related to Climate Teleconnections in the Waswanipi Area, Central Quebec, Canada. *Int. J. Wildland Fire* **2007**, *16*, 607. [CrossRef]
51. Xu, H.C. *Pinus Tabulaeformis (In Chinese)*; China Forestry Publishing House: Beijing, China, 1990; pp. 18–23.
52. Ren, P.; Rossi, S.; Gricar, J.; Liang, E.; Cufar, K. Is Precipitation a Trigger for the Onset of Xylogenesis in Juniperus Przewalskii on the North-Eastern Tibetan Plateau? *Ann. Bot.* **2015**, *115*, 629–639. [CrossRef]
53. Chen, F.; Yuan, Y. May–June Maximum Temperature Reconstruction from Mean Earlywood Density in North Central China and Its Linkages to the Summer Monsoon Activities. *PLoS ONE* **2014**, *9*, e107501. [CrossRef]
54. Liu, W.; Gou, X.; Li, J.; Huo, Y.; Yang, M.; Zhang, J.; Zhang, W.; Yin, D. Temperature Signals Complicate Tree-Ring Precipitation Reconstructions on the Northeastern Tibetan Plateau. *Glob. Planet. Change* **2021**, *200*, 103460. [CrossRef]
55. Hurrell, J.W.; Hack, J.J.; Shea, D.; Caron, J.M.; Rosinski, J. A New Sea Surface Temperature and Sea Ice Boundary Dataset for the Community Atmosphere Model. *J. Clim.* **2008**, *21*, 5145–5153. [CrossRef]
56. Gershunov, A.; Barnett, T. Interdecadal Modulation of ENSO Teleconnections. *Bull. Am. Meteorol. Soc.* **1998**, *79*, 2715–2726. [CrossRef]
57. Zhao, C.; Geng, X.; Zhang, W.; Qi, L. Atlantic Multidecadal Oscillation Modulates ENSO Atmospheric Anomaly Amplitude in the Tropical Pacific. *J. Clim.* **2022**, *35*, 3891–3903. [CrossRef]
58. Liu, Y.; Wang, Y.; Li, Q.; Song, H.; Linderholm, H.W.; Leavitt, S.W.; Wang, R.; An, Z. Tree-Ring Stable Carbon Isotope-Based May–July Temperature Reconstruction over Nanwutai, China, for the Past Century and Its Record of 20th Century Warming. *Quat. Sci. Rev.* **2014**, *93*, 67–76. [CrossRef]
59. Yin, H.; Sun, Y.; Li, M.-Y. Reconstructed Temperature Change in Late Summer over the Eastern Tibetan Plateau since 1867 CE and the Role of Anthropogenic Forcing. *Glob. Planet. Change* **2022**, *208*, 103715. [CrossRef]